JACC: ADVANCES VOL. 4, NO. 5, 2025

ORIGINAL RESEARCH

Automated, Standardized, Quantitative Analysis of Cardiovascular Borders on Chest X-Rays Using Deep Learning

June-Goo Lee, PhD,[a,*] Tae Joon Jun, PhD,[b,*] Gyujun Jeong, MS,[a] Hongmin Oh, MS,[d] Sijoon Kim, MS,[a] Heejun Kang, MS,[b] Jung Bok Lee, PhD,[b] Hyun Jung Koo, MD,[d] Jong Eun Lee, MD,[d] Joon-Won Kang, MD,[d] Yura Ahn, MD,[d] Sang Min Lee, MD,[d] Joon Beom Seo, MD,[d] Seong Ho Park, MD,[d] Min Soo Cho, MD,[e] Jung-Min Ahn, MD,[e] Duk-Woo Park, MD,[e] Joon Bum Kim, MD,[f] Cherry Kim, MD,[g] Young Joo Suh, MD,[h] Iksung Cho, MD,[i] Marly van Assen, MD,[j] Carlo N. De Cecco, MD,[j] Eun Ju Chun, MD,[k] Young-Hak Kim, MD,[e] Dong Hyun Yang, MD,[d] the ADC Investigators

ABSTRACT

BACKGROUND The analysis of cardiovascular borders (CVBs) in chest x-rays (CXRs) traditionally relied on subjective assessment and does not have established normal ranges.

OBJECTIVES The authors aimed to develop a deep learning-based method for quantifying CVBs on CXRs and to explore its clinical utility.

METHODS This study used a prevalidated deep learning to analyze CVBs. A total of 96,129 normal CXRs from 4 sites were used to establish age- and sex-specific normal ranges of CVBs. The quantified CVBs were standardized into *z*-scores for newly inputted CXRs. The clinical utility of the *z*-score analysis was tested using 44,567 diseased CXRs from 3 sites (9,964 valve disease; 32,900 coronary artery disease; 1,299 congenital heart disease; 294 aortic aneurysm; 110 mediastinal mass).

RESULTS For distinguishing valve disease from normal controls, the area under the receiver operating characteristic curve for the cardiothoracic ratio was 0.80 (95% CI: 0.80-0.80), while the combination of right atrium and left ventricle borders had an area under the receiver operating characteristic curve of 0.83 (95% CI: 0.83-0.83). Between mitral and aortic stenosis, *z*-scores of CVBs were significantly different in the left atrial appendage (1.54 vs 0.33, $P < 0.001$), carinal angle (1.10 vs 0.67, $P < 0.001$), and ascending aorta (0.63 vs 1.02, $P < 0.001$), reflecting disease pathophysiology. Cardiothoracic ratio was independently associated with a 5-year risk of death or myocardial infarction in the coronary artery disease (*z*-score ≥ 2, adjusted HR: 3.73 [95% CI: 2.09-6.64], reference *z*-score < -1).

CONCLUSIONS Deep learning-derived *z*-score analysis of CXR showed potential in classifying and stratifying the risk of cardiovascular abnormalities. (JACC Adv. 2025;4:101687) © 2025 The Authors. Published by Elsevier on behalf of the American College of Cardiology Foundation. This is an open access article under the CC BY-NC-ND license (http://creativecommons.org/licenses/by-nc-nd/4.0/).

From the [a]Biomedical Engineering Research Center, Asan Institute for Life Sciences, Asan Medical Center, Seoul, South Korea; [b]Big Data Research Center, Asan Institute for Life Sciences, Asan Medical Center, Seoul, South Korea; [c]Department of Clinical Epidemiology and Biostatistics, Asan Medical Center, Seoul, South Korea; [d]Department of Radiology, Research Institute of Radiology, Asan Medical Center, University of Ulsan College of Medicine, Seoul, South Korea; [e]Department of Cardiology, Asan Medical Center, University of Ulsan College of Medicine, Seoul, South Korea; [f]Department of Cardiothoracic Surgery, Asan Medical Center, University of Ulsan College of Medicine, Seoul, South Korea; [g]Department of Radiology, Korea University Ansan Hospital,

ISSN 2772-963X https://doi.org/10.1016/j.jacadv.2025.101687

ABBREVIATIONS AND ACRONYMS

AI = artificial intelligence
AR = aortic regurgitation
Arch = aortic arch
AS = aortic stenosis
AUC = area under the receiver operating characteristic
CAD = coronary artery disease
CCTA = coronary computed tomography angiography
CHD = congenital heart disease
CT = cardiothoracic
CVB = cardiovascular border
CXR = chest x-rays
DAO = descending aorta
LAA = left atrial appendage
LV = left ventricle
MS = mitral stenosis
PT = pulmonary trunk
RA = right atrium
SVC/AO = superior vena cava/ascending aorta
TV = tricuspid valve
VHD = valvular heart disease

Advancements in artificial intelligence (AI) have significantly changed the way chest x-rays (CXRs) are analyzed, enabling the automatic diagnosis of diseases affecting the lungs, pleura, and bones.[1-3] Recent studies have also demonstrated AI's potential in cardiovascular disease for diagnosing heart failure, predicting cardiovascular disease risks, and identifying various types of valvular diseases using CXRs.[4-8] AI systems trained to predict cardiovascular abnormalities in CXRs can provide saliency maps for their explainability, which highlight the areas focused on making diagnoses.[5,7] However, it is important to note that these heatmaps might have limitations, particularly in pinpointing specific abnormalities or diagnosing rare diseases.[9]

The cardiothoracic (CT) ratio, a traditional metric derived from CXRs, often lacks specific reference values and may not effectively reveal changes in cardiovascular borders (CVBs) such as dilatation of the aorta or pulmonary trunk (PT).[10,11] We have developed a fully automated, deep learning-based software that analyzes CVBs comprehensively.[12] This AI software might offer us an opportunity to establish precise normal ranges and detect various patterns of CVB enlargement associated with cardiovascular diseases. *Z*-scores, which represent the number of SDs a data point is from the mean of a normally distributed population, are frequently used to compare quantitative test results with reference data. The precise normal ranges of CVBs may help the standardization of all CVBs into simple *z*-scores for newly inputted CXRs. We therefore conducted the ADC ("Automated Diagnosis of Cardiovascular abnormalities using chest x-ray") study to develop a deep learning-based method for quantifying CVBs on CXRs and to explore its clinical utility.

METHODS

STUDY DESIGN. The ADC was a retrospective, multicenter study initiated by investigators and included 140,696 CXRs from 3 academic centers in 2 countries (South Korea, the United States), as well as 2 public U.S. data sets.[13,14] The study protocol received ethical approval from the Institutional Review Boards of all participating institutions, and informed consent was waived for all participants (Asan Medical Center, Seoul, Korea; 2023-1001; Severance Hospital, Seoul, Korea; 4-2020-0628; Emory University, Atlanta, Georgia, USA; STUDY00005513). The study design is summarized in the **Central Illustration**. Briefly, we utilized a prevalidated deep learning model to automatically delineate CVBs on 96,129 normal CXRs.[12] This deep learning-based analysis enabled the quantification of CVBs and the establishment of age- and sex-specific normal ranges for both Korea and the United States. These normal ranges facilitated the standardization of individual CVBs into simple *z*-scores for newly inputted CXRs (**Figure 1**). The clinical utility of the *z*-score mapping was evaluated across various disease groups, including valvular heart disease (VHD), coronary artery disease (CAD), congenital heart disease (CHD), aortic aneurysm, and mediastinal mass.

STUDY COHORTS. The study cohorts consisted of 140,696 unique patients and CXRs as summarized in **Figure 2**. The normal cohorts (**Figure 2A**) used to establish reference ranges of CVBs encompassed data from Asan Medical Center (Seoul, Korea) labeled as "Normal Korean" (n = 71,493) and 3 American data sets collectively labeled as "Normal American" (n = 24,636). The data set from Asan Medical Center spanned from 2002 to 2016, including 428,000 individuals who underwent both CXR and transthoracic echocardiography within a 6-month period, with 71,493 meeting the criteria for normality in both tests (Supplemental Table 1, Supplemental Figure 1). Data extraction and analysis were performed by the Big

Ansan, South Korea; [h]Department of Radiology, Severance Hospital, Yonsei University College of Medicine, Seoul, South Korea; [i]Division of Cardiology, Severance Hospital, Yonsei University College of Medicine, Seoul, South Korea; [j]Translational Laboratory for Cardiothoracic Imaging and Artificial Intelligence, Emory University School of Medicine, Atlanta, Georgia, USA; and the [k]Department of Radiology, Seoul National University Bundang Hospital, Seongnam, South Korea. *These authors contributed equally to this work.

Manuscript received November 3, 2024; revised manuscript received February 19, 2025, accepted February 21, 2025.

CENTRAL ILLUSTRATION **Automated, Standardized, Quantitative Analysis of Cardiovascular Borders on Chest X-Rays Using Deep Learning**

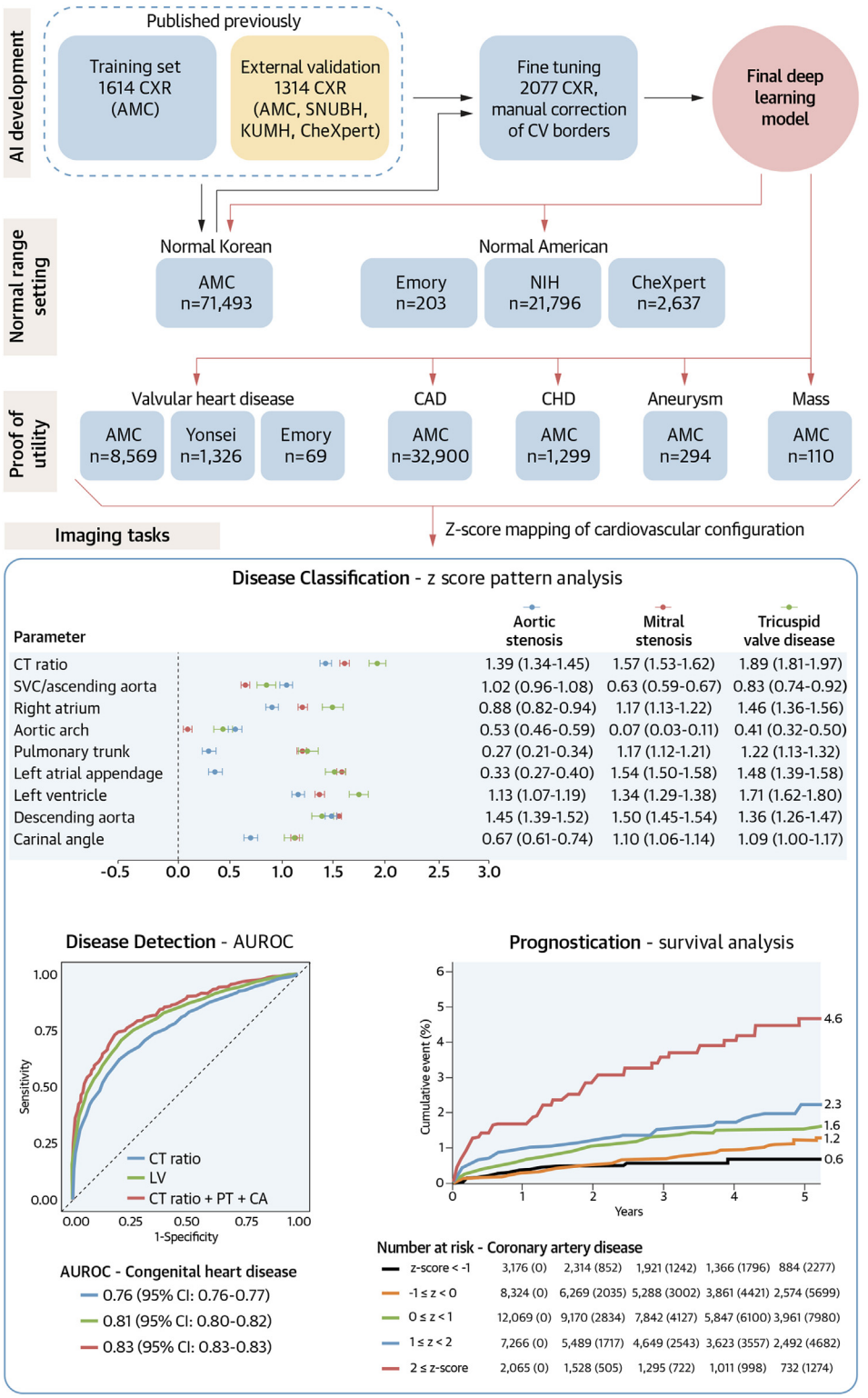

Lee J-G, et al. JACC Adv. 2025;4(5):101687.

AUROC = area under the receiver operating characteristic curve; CAD = coronary artery disease; CHD = congenital heart disease; other abbreviations as in Figures 1, 3, and 5.

FIGURE 1 Z-Score Mapping Process for Cardiovascular Borders in Chest X-Rays

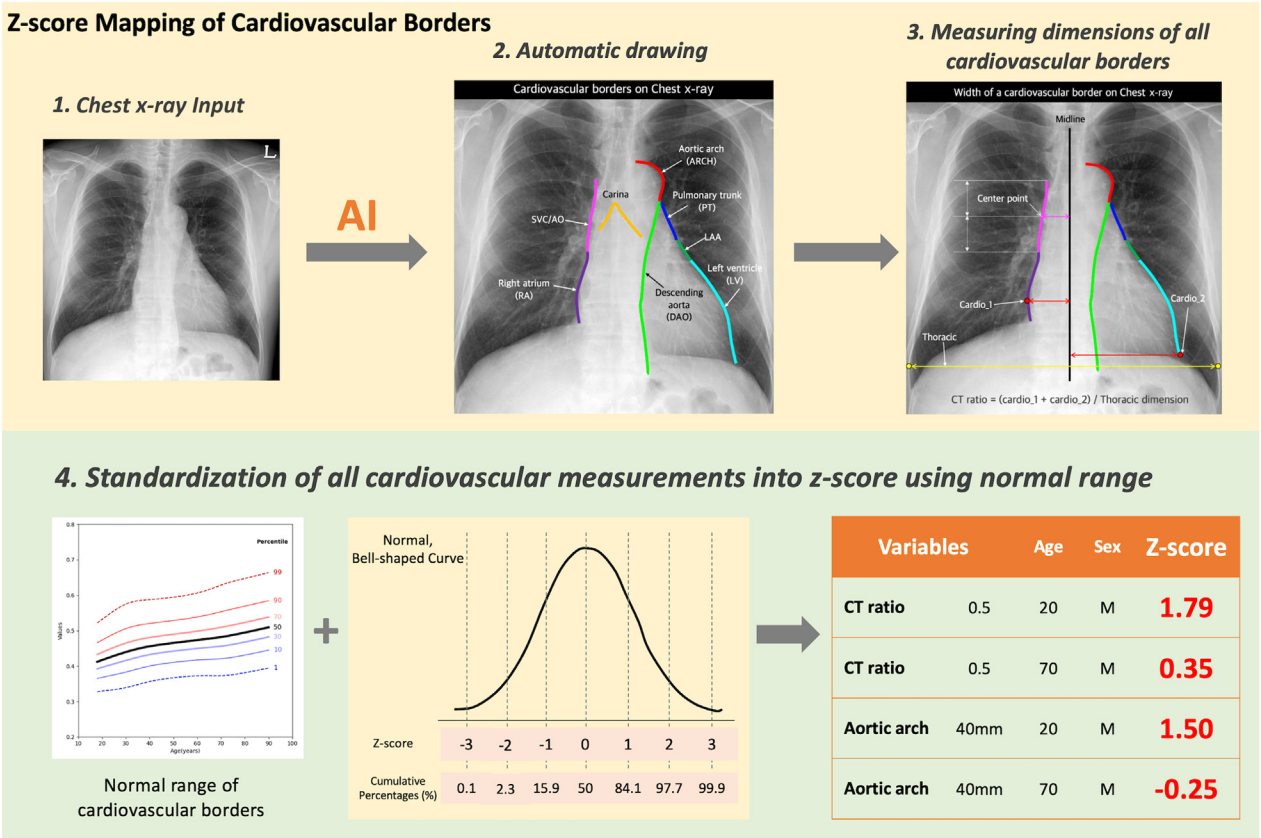

1. A standard posterior-anterior chest x-ray is used as the input for the AI analysis. 2. AI algorithms automatically identify and delineate the CVBs on the chest x-ray. 3. The software measures the dimensions from the midline to key points on the CVBs to calculate the cardiothoracic (CT) ratio and the dimensions of individual CVBs. The width of each CVB is defined as the distance between the center points of each CVB and the midline of the CXR. The CT ratio was calculated by dividing the maximum width of the right lower CVB (corresponding to the right atrium) and the left lower cardiovascular border (corresponding to the left ventricle) by the maximal horizontal thoracic diameter. 4. The measurements are then standardized into *z*-scores based on the normal range, allowing for comparison according to age and sex. AI = artificial intelligence; CVB = cardiovascular border; CXR = chest x-ray; LAA = left atrial appendage; SVC/AO = superior vena cava/ascending aorta.

Data Research Center at Asan Medical Center utilizing the CardioNet database, a meticulously curated database integrated within the electronic health records.[15] The selection criteria for normal CXRs involved a comprehensive review of structured echocardiography records, radiological reports, and International Classification of Diseases Codes, carefully excluding any cases indicative of cardiac, pleuropulmonary diseases, or skeletal anomalies such as scoliosis. The Normal American data set was derived from 2 publicly accessible data sets—one from the National Institutes of Health Clinical Center (NIH subgroup)[13] and another from Stanford University Hospital (CheXpert Subgroup)[14]—as well as a data set from Emory University Medical Center, Atlanta, USA (Emory Subgroup) (Supplemental Table 2). For these data sets, CXRs without lung lesions and cardiomegaly were chosen after evaluations of structured radiological reports and labels. Individuals in the Emory subgroup were selected based on having normal results in both CXR and echocardiography.

The study enrolled 5 disease groups (**Figure 2B**) including the VHD group (n = 9,964), patients evaluated for CAD with coronary computed tomography angiography (CCTA) without any other heart disease (CAD group, n = 32,900),[16] individuals who had undergone surgery for atrial or ventricular septal defects (CHD group, n = 1,299), patients confirmed with thoracic aortic aneurysms by computed tomography (aneurysm group, n = 294), and patients with biopsy-proven mediastinal masses (mass group, n = 110). The VHD group was recruited from 3 institutions: Asan

FIGURE 2 Study Cohort Construction

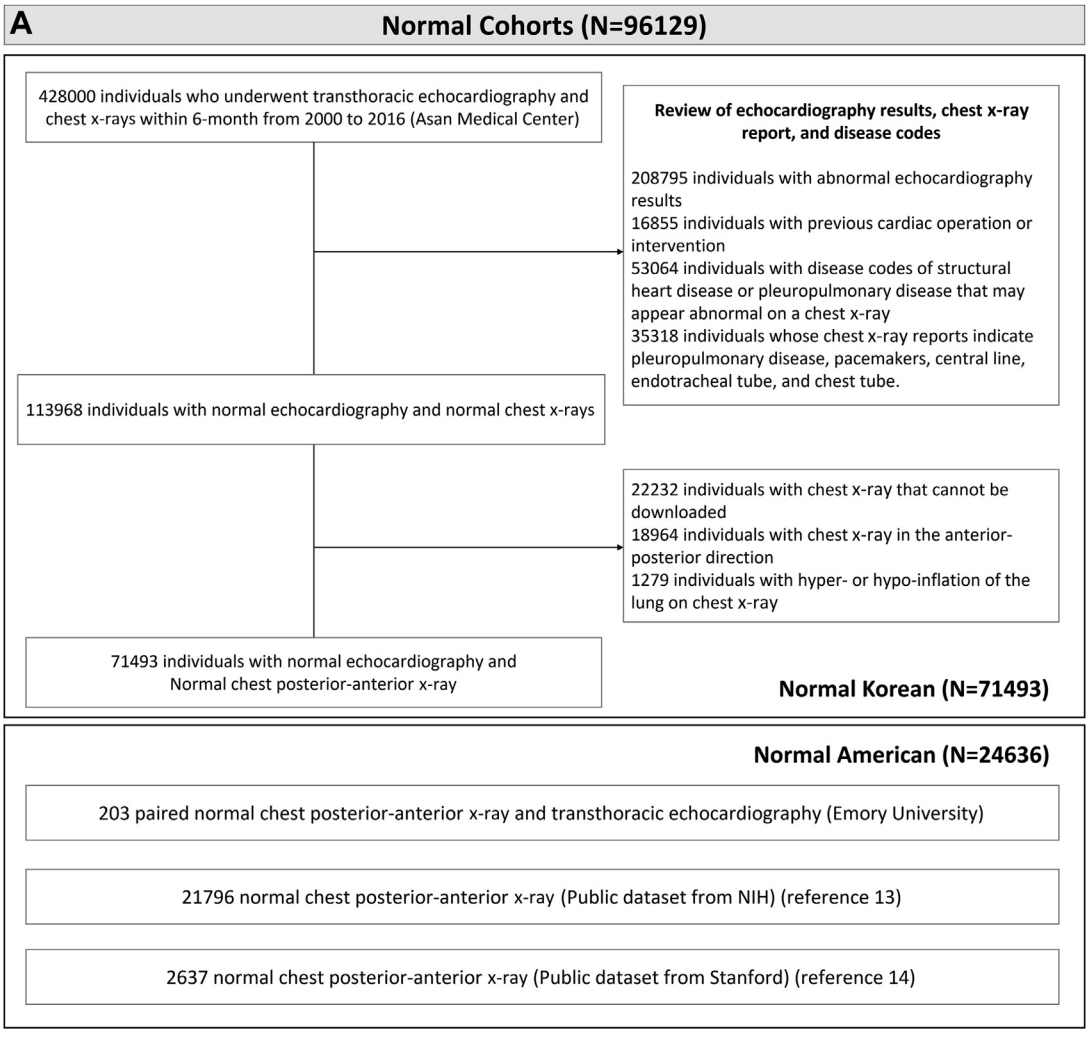

(A) Normal cohort. (B) Disease cohorts.

Continued on the next page

Medical Center, Severance Hospital, and Emory University Medical Center, while the remaining disease groups (CAD, CHD, aneurysm, and mass) were recruited from Asan Medical Center. Further details about each disease subgroup are provided in the Supplement (Supplemental Tables 3 to 5, Supplemental Figure 2). The VHD group included patients with moderate or severe VHD who were identified using a combination of the International Classification of Diseases-10 codes and structured echocardiography reports and was further categorized according to the dominant or most severe valve disease into the aortic stenosis (AS), aortic regurgitation (AR), mitral stenosis (MS), mitral regurgitation, and tricuspid valve (TV) subgroups. The CAD group data, which was used for the prognostication testing in this study, included a median follow-up of 2.9 years (IQR: 1.0-4.5 years) and was segmented into significant CAD subgroups based on >50% stenosis observed in CCTA.[16] The primary long-term clinical outcome was the composite of death from any cause or myocardial infarction at 5 years after CCTA.[16] The aneurysm group was composed of patients with an ascending aorta >4.5 cm or a descending aorta (DAO)/arch larger than 4 cm as confirmed by CT. The mass group retrospectively

FIGURE 2 Continued

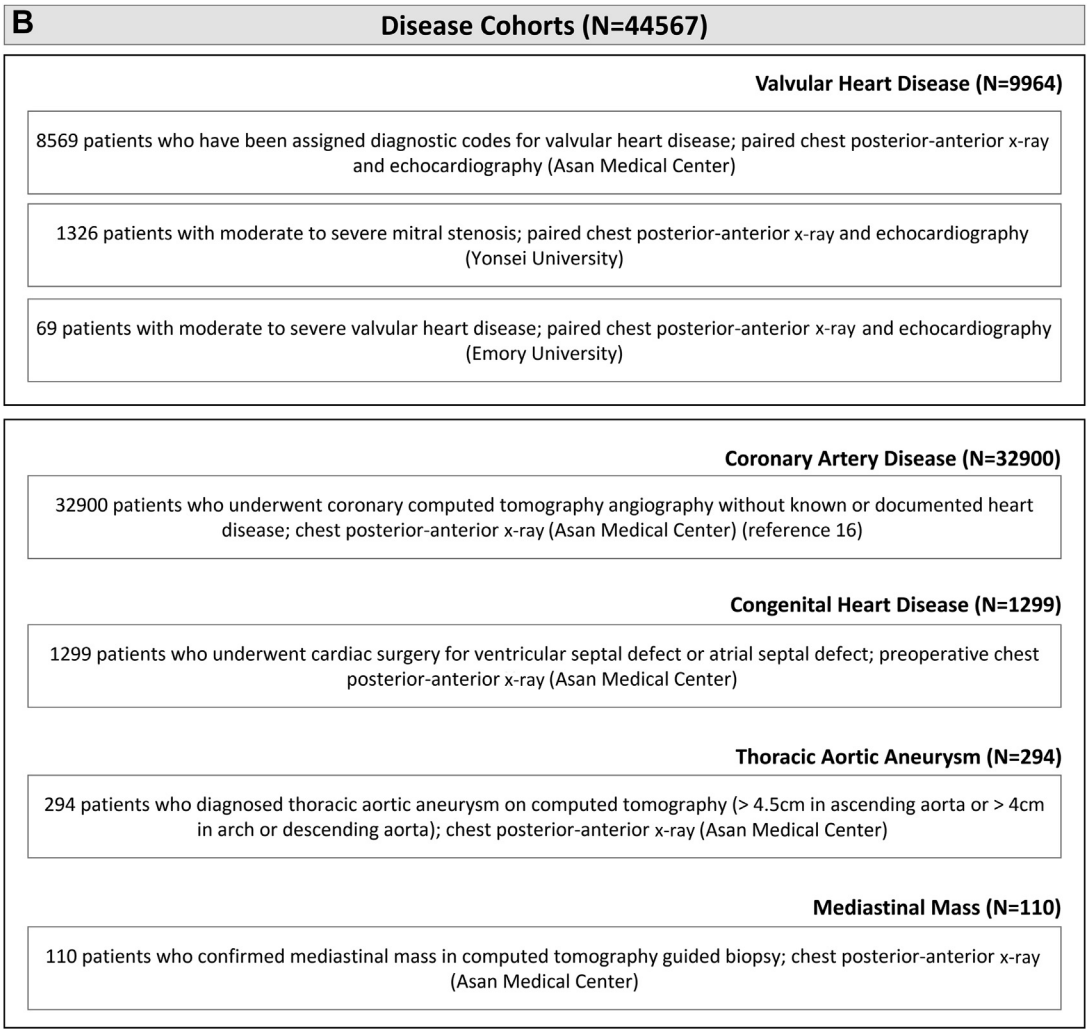

enrolled patients with mediastinal masses confirmed by CT-guided biopsy.

AI MODEL. The CVB analysis software has been previously validated against multi-institutional data sets.[12] This AI software automatically delineates each CVB when a CXR is inputted. The width of each CVB was calculated by measuring the distance from the midline of the CXR to the centerpoint of the height (**Figure 1**). Each CVB was named based on its normal anatomical location as follows: superior vena cava/ascending aorta (SVC/AO), right atrium (RA), aortic arch (Arch), PT, left atrial appendage (LAA), left ventricle (LV), DAO, and the carinal angle (the angle between the lower borders of the right and left main bronchi). The definitions of each CVB are detailed in Supplemental Table 6. For CVB analysis, only CXRs taken in the posteroanterior direction with the patient standing and with proper lung inflation were analyzed. Our AI model automatically excludes inappropriate CXRs, such as anteroposterior/lateral images or suboptimal lung inflation images (eg, hyperinflation or hypoinflation or asymmetric lung areas). Detailed information on the deep learning algorithm and imaging analysis workflow is provided in the Supplemental Methods (Supplemental Figure 3). This AI model is available for external validation and public use via our noncommercial research website (www.adcstudy.com), which provides real-time CXR analysis capabilities (Supplemental Figure 4).

ANALYSIS OF AI MEASUREMENTS. While most of the extracted CVB metrics approximated a symmetrical distribution, some variations in kurtosis across

TABLE 1 Baseline Characteristics and Measurements of Echocardiography and Chest X-Ray

	Normal Korean (n = 71,493)	Normal American (n = 24,636)	VHD (n = 9,964)	CAD (n = 32,900)	CHD (n = 1,299)	Aneurysm (n = 294)	Mass (n = 110)
Demographics							
Age, y	54.2 ± 11.4	46.3 ± 16.5	56.9 ± 15.4	57.2 ± 10.0	46.5 ± 14.2	59.4 ± 13.9	47.4 ± 18.4
Male	42,932 (60.1)	13,566 (55.1)	4,304 (43.2)	20,047 (60.9)	482 (37.1)	214 (72.8)	54 (49.1)
Height, cm	164.1 ± 8.7	NA	160.5 ± 9.2	164.4 ± 8.7	161.8 ± 9.1	167.2 ± 10.1	90.7 ± 29.4
Weight, kg	63.8 ± 10.7	NA	60.1 ± 10.9	66.6 ± 11.3	59.5 ± 11.3	67.6 ± 12.4	65.7 ± 13.3
Body mass index, kg/m^2	23.6 ± 2.9	29.3 (9.2)[a]	23.4 ± 3.4	24.5 ± 3.0	22.6 ± 3.3	24.1 ± 3.7	24.3 ± 3.9
Body surface area, m^2	1.70 ± 0.18	NA	1.64 ± 0.18	1.74 ± 0.18	1.63 ± 0.19	1.77 ± 0.20	1.94 ± 1.97
Echocardiography							
LV EDV index, mL/m^2	83.4 ± 20.8	NA	105.1 ± 49.7	89.2 ± 26.4	87.4 ± 29.7	109.3 ± 45.9	90.7 ± 29.4
LV ESV index, mL/m^2	30.8 ± 8.6	NA	45.8 ± 32.5	33.5 ± 13.0	34.7 ± 15.5	47.1 ± 32.4	34.2 ± 16.7
LV ejection fraction, %	63.1 ± 3.7	61.3 (4.98)[a]	59.4 ± 10.1	62.6 ± 8.3	60.9 ± 7.1	59.0 ± 9.4	62.8 ± 6.2
Ascending aorta, mm	32.1 ± 3.5	NA	32.9 ± 7.0	33.1 ± 6.7	31.4 ± 4.4	36.9 ± 5.3	32.4 ± 4.5
Chest x-ray							
Acceptance rate, %	98.2 (71,493/72,772)	96.8 (24,636/25,444)	96.2 (9,964/10,357)	95.5 (32,900/34,446)	97.3 (1,299/1,335)	89.9 (294/327)	98.2 (110/112)
CT ratio	0.48 ± 0.05	0.47 ± 0.06	0.56 ± 0.08	0.49 ± 0.06	0.55 ± 0.08	0.56 ± 0.07	0.49 ± 0.05
SVC/AO, mm	28.4 ± 6.8	29.3 ± 8.5	32.6 ± 9.4	29.7 ± 7.2	29.8 ± 9.2	37.8 ± 11.3	36.3 ± 12.4
Right atrium, mm	39.1 ± 7.8	41.4 ± 9.4	46.2 ± 11.3	40.8 ± 8.2	44.1 ± 12.4	48.0 ± 11.9	40.8 ± 8.7
Aortic arch, mm	38.3 ± 6.7	35.3 ± 8.3	39.4 ± 8.2	39.5 ± 6.8	37.2 ± 8.0	52.6 ± 14.0	40.9 ± 9.4
Pulmonary trunk, mm	38.5 ± 6.4	37.8 ± 7.9	43.3 ± 8.6	39.8 ± 6.8	47.0 ± 9.2	46.2 ± 10.4	45.3 ± 10.1
Left atrial appendage, mm	46.4 ± 7.3	46.7 ± 9.1	53.9 ± 10.2	48.1 ± 7.8	58.1 ± 10.6	54.1 ± 10.8	53.2 ± 10.0
Left ventricle, mm	84.6 ± 10.5	85.6 ± 14.2	96.6 ± 14.0	88.7 ± 11.3	98.7 ± 14.4	101.9 ± 14.2	85.9 ± 10.9
Descending aorta, mm	33.3 ± 8.6	29.1 ± 9.5	42.2 ± 11.2	36.2 ± 9.4	35.0 ± 11.5	56.3 ± 16.0	35.2 ± 9.5
Carinal angle, degree	71.1 ± 8.7	72.3 ± 9.6	79.3 ± 11.2	72.1 ± 9.6	77.7 ± 11.1	80.7 ± 12.1	77.9 ± 8.9

Values are mean ± SD, n (%), or % (n/N). [a]The data derived from the 203 normal subjects from Emory University.

CAD = coronary artery disease; CHD = congenital heart disease; CT = cardiothoracic; EDV = end-diastolic volume; ESV = end-systolic volume; LV = left ventricle; NA = not available; SVC/AO = superior vena cava/ascending aorta; VHD = valvular heart disease. Acceptance rate represents the proportion of inputted chest posteroanterior x-rays that were successfully analyzed and found to be free of lung hyperinflation or hypoinflation. Body mass index and LV ejection fraction in the Normal American from Emory University subgroup.

different metrics as well as skewness in DAO were noted (Supplemental Figures 5 and 6). To account for these discrepancies, each CVB metric underwent a transformation to a Box-Cox normal distribution using Generalized Additive Models for Location, Scale, and Shape.[17] Percentile curves were plotted for individual measurements, and *z*-scores were computed.[17,18] Then, the dimensions of each CVBs were standardized into *z*-scores.

STATISTICAL ANALYSIS. Continuous variables are presented as means and SDs, while categorical variables are presented as counts and percentages. *Z*-scores for each disease group are shown along with their means and 95% CIs. The diagnostic performance of CVB metrics in detecting specific diseases was evaluated using the area under the receiver operating characteristic (AUC), calculated with the pROC package (version 1.18.5) and included sensitivity, specificity, accuracy, positive predictive value, and negative predictive value with cutoff point determined by the maximum Youden index. Diagnostic performance was assessed for the VHD, CAD, and CHD groups, as well as for subgroups within VHD. For each disease category, a control group 3 times the size of the disease group was randomly selected from the Normal Korean cohort. Additionally, we performed 5-fold cross-validation to validate the model's performance across multiple splits, reducing bias and enhancing generalizability. Multivariable logistic regression analysis was used to identify CVBs significantly associated with the presence of disease. Only CVB metrics that demonstrated a P value <0.01 in univariable analysis and had low intercorrelations ($r < 0.20$) were included in the multivariable analysis. The multivariable model was developed using 60% of the randomly divided data and validated using the remaining 40%.

For the CAD group, Kaplan-Meier survival analyses were conducted using the survival package (version 3.5.5), and Cox proportional hazards regression models were used to examine the relationship between CVB *z*-scores and patient outcomes, independent of known cardiovascular risk factors. These analyses focused on the composite outcome of death from any cause or myocardial

FIGURE 3 Age-Related Percentile Curves for Cardiovascular Borders in Normal Chest X-Ray

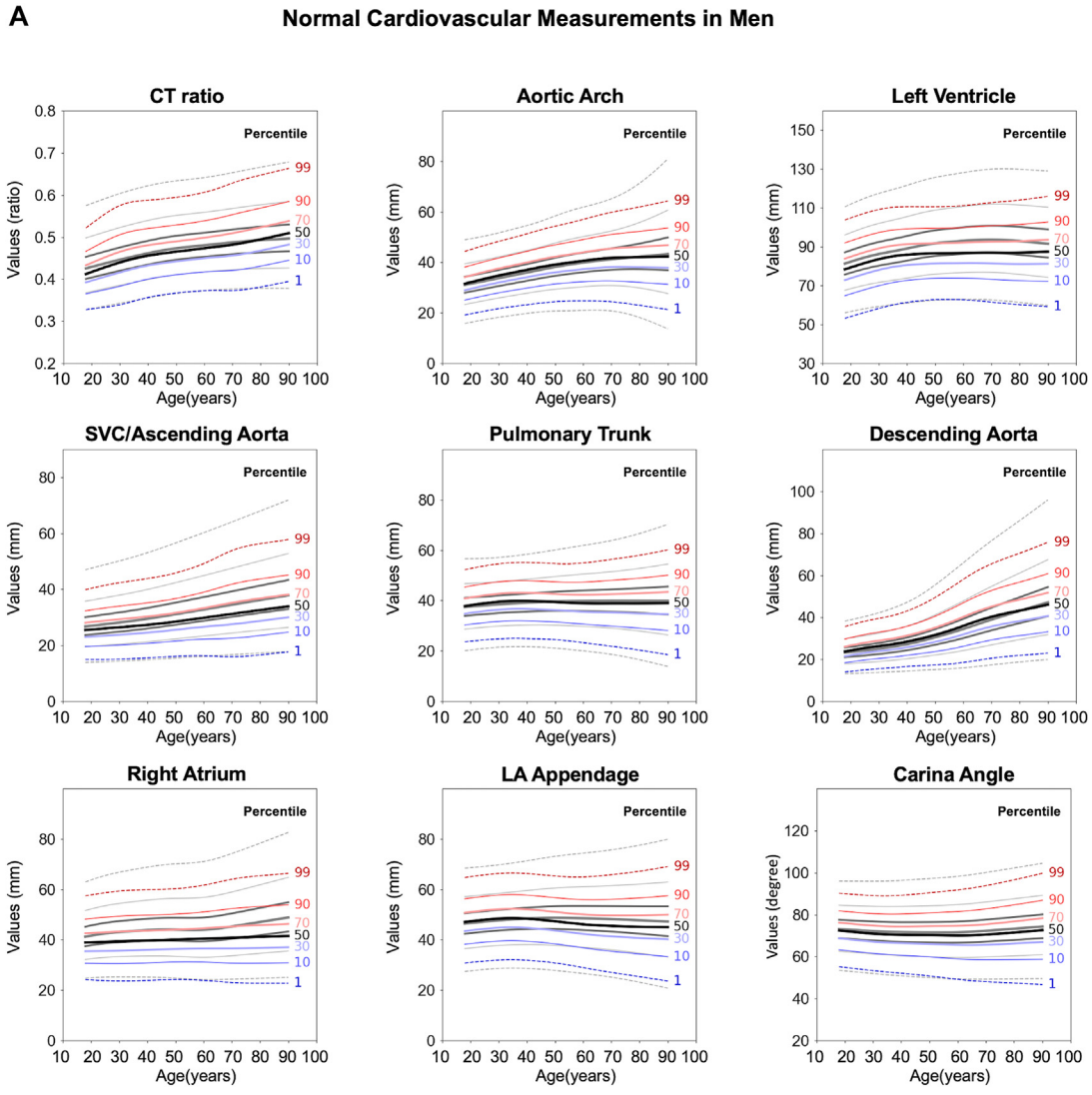

Percentile graphs of cardiovascular borders according to age for normal men (A) and women (B). The data in red or blue represent Normal Korean individuals, and the data overlapped in gray represent that of Normal Americans. Note that the age range of 20 to 100 years includes extrapolated values at the extremes CT = cardiothoracic; LA = left atrium; other abbreviation as in Figure 1.

Continued on the next page

infarction following CCTA. The Framingham Risk Score, body mass index, the presence of diabetes mellitus, estimated glomerular filtration rate, symptoms at CCTA, and obstructed CAD (defined as ≥50% diameter stenosis) on CCTA were incorporated into the multivariable regression models, consistent with previously published results.[16] The CVB *z*-scores were categorized as follows: *z*-score <−1, −1 ≤ z-score <0, 0 ≤ *z*-score <1, 1 ≤ *z*-score <2, and *z*-score ≥2.

RESULTS

STUDY POPULATION. The study population comprised 96,129 individuals in the normal cohorts and 44,567 patients in the disease cohorts (Table 1, Figure 2). The mean age ranged from 46.5 years in the CHD group to 59.4 years in the aneurysm group. The VHD group included 1432 AS (14.4%), 1756 AR (17.6%), 2897 MS (29.1%), 2971 mitral regurgitation (29.8%), 785 TV disease (7.9%), 72 pulmonary valve disease (0.7%),

FIGURE 3 Continued

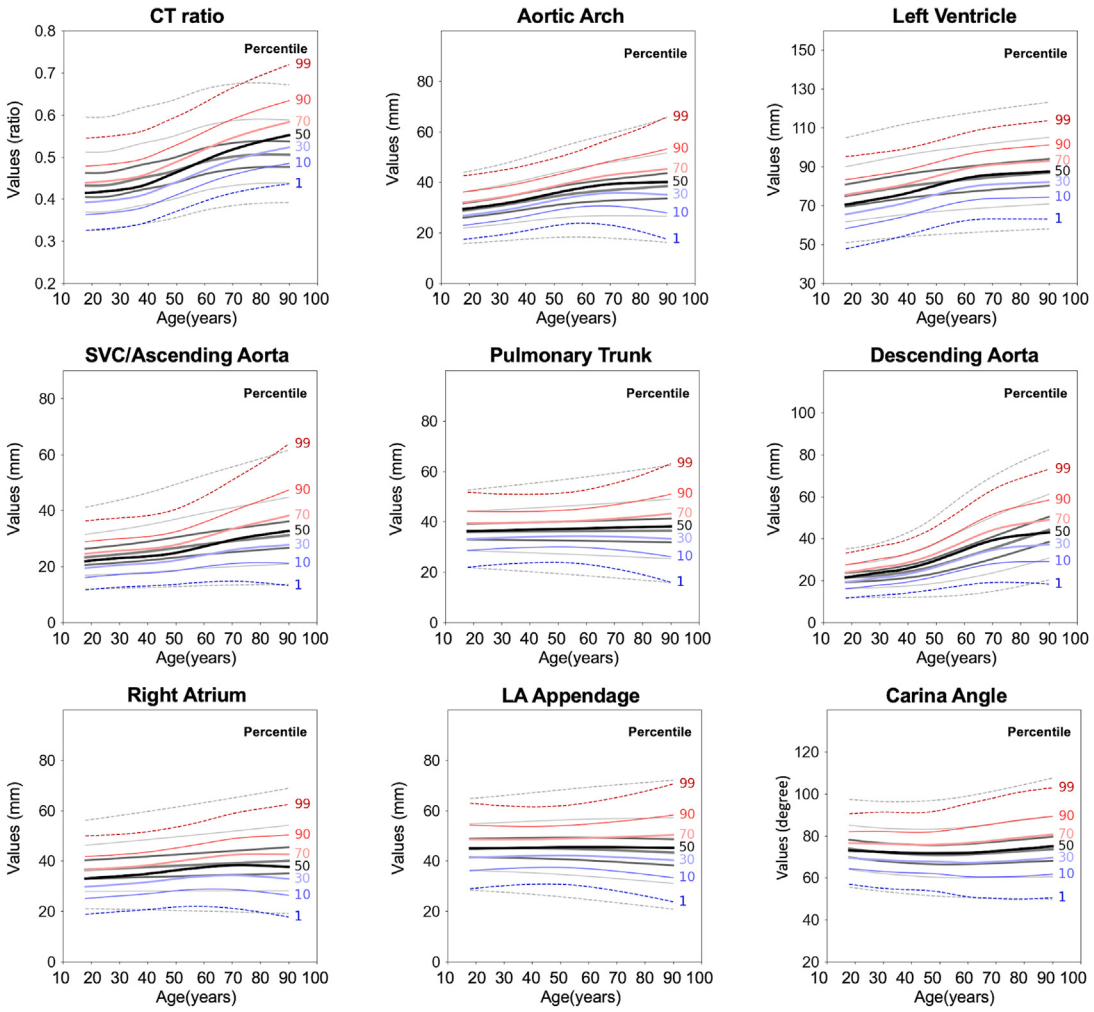

and 51 multivalve disease (0.5%) cases (Supplemental Table 7). Echocardiography results show LV ejection fraction and other cardiac dimensions, with disease groups often showing enlarged measurements compared to normal.

NORMAL RANGE OF CVBs. Supplemental Table 8 summarizes the normal ranges for CVBs on posteroanterior CXR for different age groups in both Korean and American populations according to sex. **Figure 3** presents a set of graphs depicting age-related percentile curves for various CVBs in normal individuals; detailed graphs for Normal American and Korean cohorts were provided in the Supplemental Figures 7 to 10. For both populations, the CT ratio tends to increase with age; similarly, the diameters for SVC/AO, RA, Arch, LV, and DAO also increased with age, reflecting physiological changes in the cardiovascular system as age advances. Intercohort comparisons revealed slightly larger CVBs in the American group, differences that were mitigated after adjusting for CT ratio.

***Z*-SCORES OF CVBs IN DISEASE GROUPS.** In the analysis of disease groups, *z*-scores for CVB were generally elevated, with the VHD and CHD groups displaying significantly higher *z*-scores compared to the CAD group (**Figure 4**, Supplemental Table 9). Specifically, the mean *z*-scores for the CT ratio were 0.39 in CAD, 1.27 in CHD, and 1.40 in VHD. **Figure 4**

FIGURE 4 Comparative *Z*-Score Forest Plot for Disease Classification

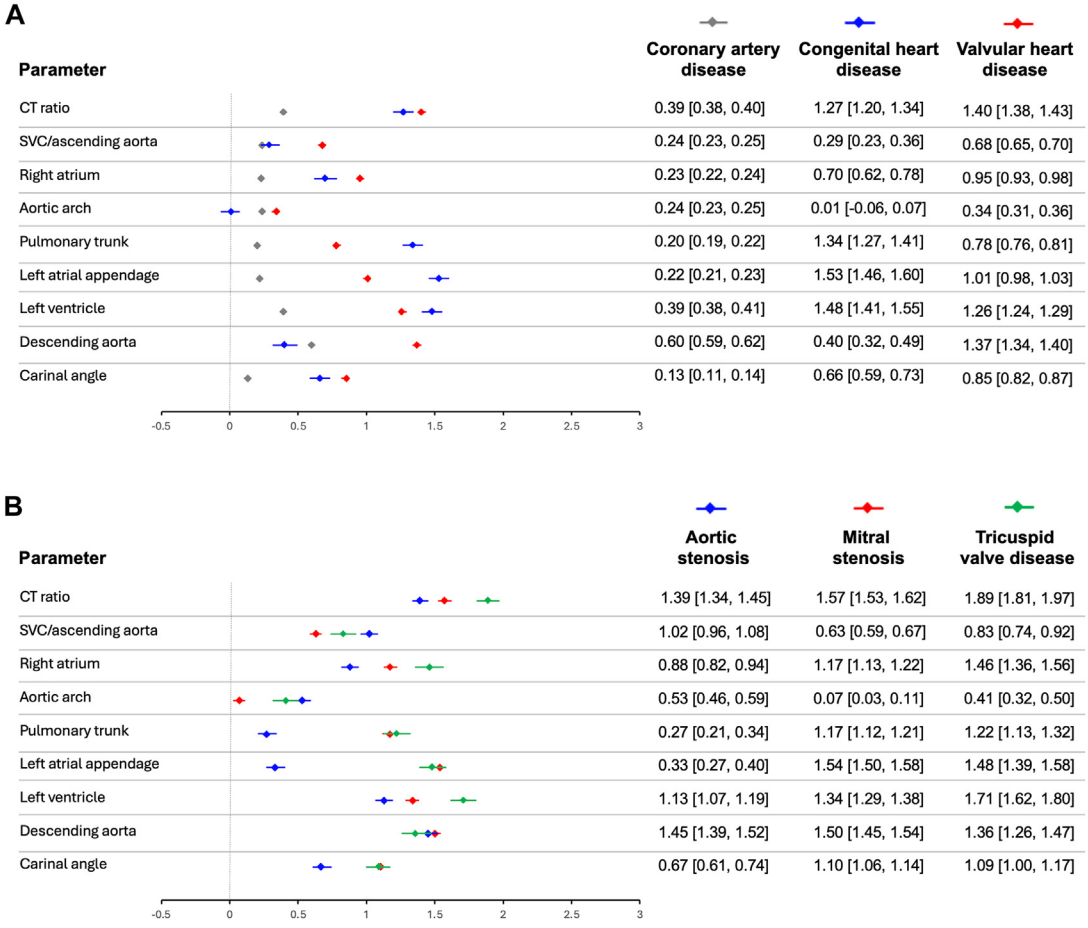

Each parameter is represented by a horizontal line, with data points indicating the mean *Z*-score and error bars showing 95% CIs. (A) Comparison across different disease groups: coronary artery disease, congenital heart disease, and valvular heart disease. (B) Comparison across specific valvular heart disease: aortic stenosis, mitral stenosis, and tricuspid valve disease. Abbreviations as in Figures 1 and 3.

highlights the variations in *z*-scores across diseases, showcasing the disease-specific changes in CVB parameters. MS, often accompanied by left atrial enlargement, showed marked increases in the LAA (*z*-score = 1.54) and carinal angle (*z*-score = 1.10) as a result of the left atrial pushing upward; this was in marked contrast to AS where the increase in the SVC/AO (*z*-score = 1.02) indicated dilation of the ascending aorta. In CHD, including atrial or ventricular septal defects, the *z*-score of the Arch (0.01) was relatively low, reflecting the reduced cardiac output of the left heart due to left-to-right shunt disease. The aortic aneurysm group showed significant increases in the arch (1.95) and DAO (2.65) *z*-scores, indicating aneurysmal changes. Mediastinal mass conditions also demonstrated elevated *z*-scores, especially for the SVC/AO (1.04) and the PT (1.03), which may indicate a mass shadow or compression caused by the tumor.

DIAGNOSTIC PERFORMANCE. The diagnostic evaluation of CVBs highlighted the CT ratio *z*-score as a robust metric across VHD, CAD, and CHD groups (Figure 5). The AUC for detecting VHD using the CT ratio reached 0.80 (95% CI: 0.80-0.80), which was increased to 0.83 (95% CI: 0.83-0.83) when combined with RA and LV metrics. CHD detection benefited from a CT ratio AUC of 0.76 (95% CI: 0.76-0.77), which improved to 0.83 (95% CI: 0.83-0.83) when PT and carinal angle were added. Among the subgroups of VHD, TV disease detection had the highest AUC of 0.88 (95% CI: 0.87-0.88) using the CT ratio. Detailed information on demographics, AUC, sensitivity,

FIGURE 5 **Performance of the *Z*-Score Mapping of Cardiovascular Borders for the Detection of Cardiovascular Disease**

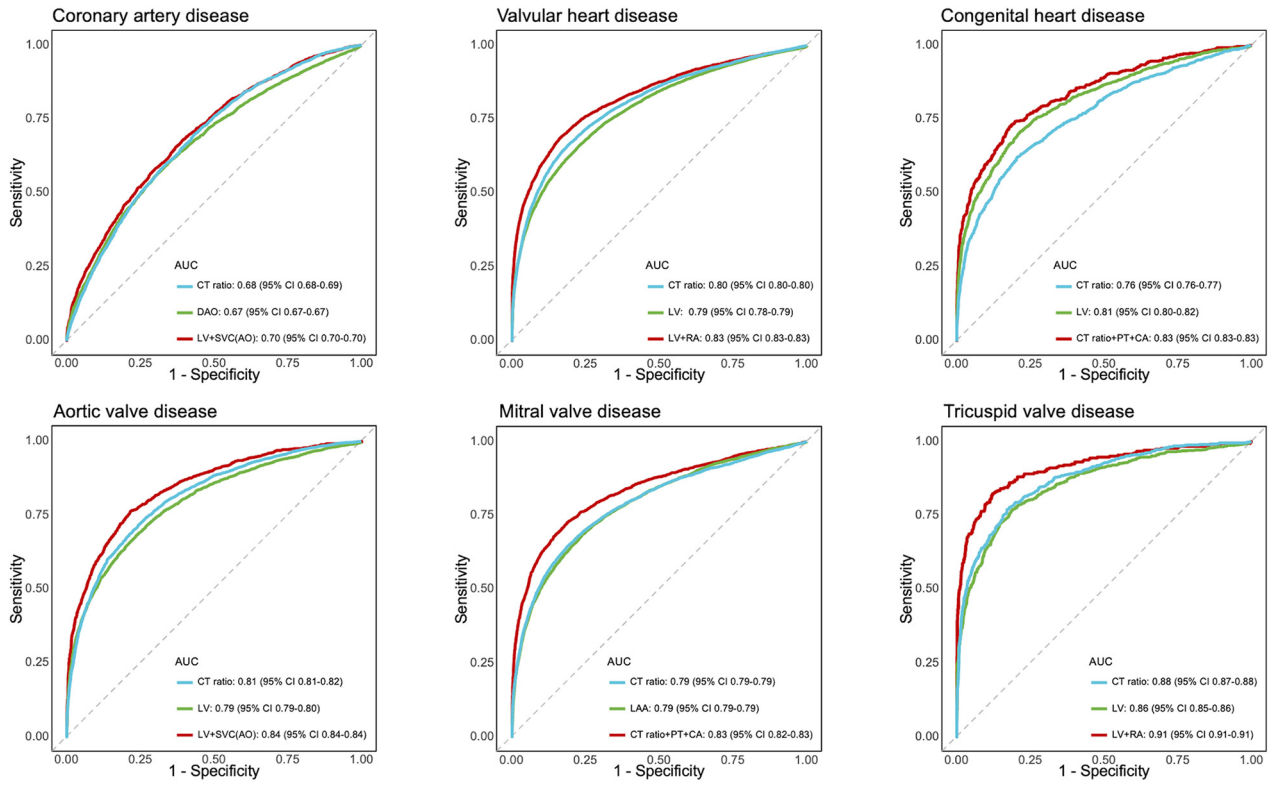

AUC = area under the receiver operating characteristic curve; CA = carinal angle; DAO = descending aorta; LAA = left atrial appendage; LV = left ventricle; PT = pulmonary trunk; RA = right atrium; other abbreviations as in **Figures 1 and 3**.

specificity, cutoff, positive predictive value, and negative predictive value is provided in Supplemental Tables 10 to 17.

PROGNOSTIC VALUE. In the cohort of 32,900 CAD patients, there were 390 (1.18%) instances of all-cause death or myocardial infarctions. CT ratio *z*-scores indicated an increasing risk with higher scores (**Figure 6**). Patients with a CT ratio *z*-score of 2 or higher were at a significantly elevated risk (adjusted HR: 3.73; 95% CI: 2.09-6.64), showing a higher percentage of cumulative events (4.6% vs 0.6%, $P < 0.001$) over 5 years compared to the reference group with a *z*-score less than −1 (HR: 1.00). Elevated risks were also observed with higher *z*-scores (≥2) for SVC/AO, RA, DAO, and carinal angle, while the Arch, PT, LAA, and LV *z*-scores not reaching statistical significance (Supplemental Table 18, Supplemental Figures 11 to 18).

CASE EXAMPLES. We presented 8 CXR case examples (Supplemental Figures 19 to 26), illustrating the application of *z*-score mapping in diagnosing various cardiomediastinal diseases. The cases span a range of conditions, including AS, MS, AR, atrial septal defect, aortic aneurysms, and mediastinal masses.

DISCUSSION

In the ADC study, we established normal values for CVBs and introduced a new methodology for utilizing CXRs in cardiovascular disease diagnosis. Our main findings are as follows. First, *z*-score mapping for CVBs was feasible in disease diagnosis. In certain cases, combining different CVBs enhanced diagnostic accuracy beyond the CT ratio. Second, variations in *z*-scores, reflecting the underlying disease pathophysiology, indicate that CXRs could be useful in classifying diseases, such as distinguishing between aortic and mitral valve diseases. As demonstrated through our case presentations, the changes in individual CVB *z*-scores may be correlated with the pathophysiological changes observed in patients'

FIGURE 6 All-Cause Death or Myocardial Infarction Stratified by Cardiothoracic Ratio *Z*-Score in the Coronary Artery Disease Group, All-Cause Death or Myocardial Infarction Were Stratified by *Z*-Score Categories of the CT Ratio

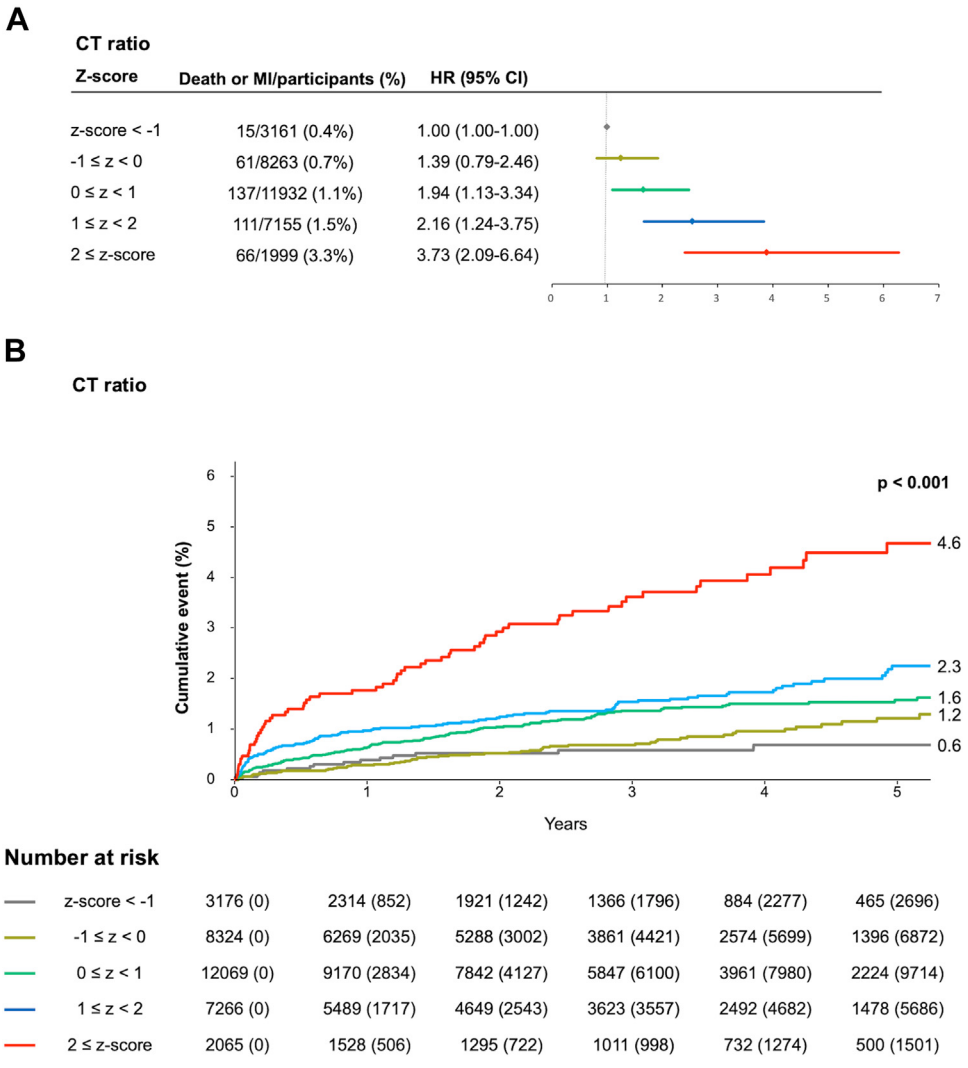

Adjusted HRs were compared with the lowest *Z*-score group (<−1). (A) Percent of death or myocardial infarction and adjusted HR increased across ascending *Z*-score categories. (B) Cumulative event rate for each *Z*-score category of the CT ratio during a follow-up duration of 5 years. Abbreviation as in **Figure 3**.

echocardiograms or CT scans. The *z*-score mapping allows for a more objective and quantifiable method of interpretation compared to traditional approaches to CXR analysis. Lastly, measures of CVB, including the CT ratio, showed potential in predicting clinical outcomes, adding value to traditional risk scoring systems.

Regarding the quantitative analysis of CXR, previous studies have focused on automatically extracting the CT ratio [19-22] and biological age [23] from CXRs using AI. As demonstrated in the ADC study, the variability of the CT ratio's normal values based on age and sex indicates limitations in applying a single cutoff 0.5. Moreover, conditions such as PT and ascending aortic dilatation cannot be adequately assessed by the CT ratio alone. The significance of this ADC study lies in standardizing various CVBs into a single parameter of *z*-score, not just the CT ratio, particularly showing some success in making differential diagnoses that were not previously possible with the CT ratio. Extracting biological age from CXR has shown promising prognostic value when added to existing

cardiovascular risk matrices, offering a potential new utility for CXR.[23] Since, CXR-derived biological age and CVB *z*-scores are numerical data and likely independent, combining them could offer potential for clinical practice and research applications.

The use of "end-to-end" supervised learning, where AI directly learns from CXRs with abnormalities compared to a control group, is a widely adopted approach in current AI research. This method has been extensively applied in the field of cardiovascular disease to predict conditions such as acute chest pain syndrome,[24] aortic dissection,[25] LV systolic dysfunction,[6] structural LV disease,[7] VHD,[5] AS,[26] and atrial fibrillation,[27] using CXRs. Other studies have also tried to predict the 10-year risk for major adverse cardiovascular events using CXRs.[8] These studies often employ saliency maps to improve the explainability of AI, indicating the specific areas of the image that the AI prioritized to reach its decision. However, saliency maps can struggle with the precise localization of abnormalities and may pose interpretative challenges when applied to diseases not included in the algorithm's training.[9] *Z*-score mapping, by providing interpretable numerical values independent of specific diseases, can help overcome these limitations, offering broader applicability across various cardiomediastinal conditions. This advancement may offer a modernized approach to interpreting CXRs, aligning with clinicians' preference for quantifiable metrics, such as blood tests and echocardiographic parameters. Moreover, this numerical approach facilitates a more objective comparison during the follow-up of CXRs, making it easier to interpret changes over time in a patient's condition.

For the utilization of *z*-score mapping of CXR in real-world clinical practice, it is crucial to establish the most appropriate clinical application scenarios. For example, *z*-score mapping of CXRs could serve as a gatekeeper before proceeding to more costly and complex tests such as echocardiography. Another promising scenario could involve using *z*-score mapping of CXRs as a screening tool to detect left-to-right shunt diseases before they progress to irreversible pulmonary hypertension. Such applications could significantly enhance the utility of CXR, providing a cost-effective, accessible, and noninvasive method. Particularly, using CXRs for VHD or CHD in screening scenarios could be a viable alternative in underdeveloped countries where health care infrastructure is insufficient.[28]

This study has the following limitations: First, the CVB analysis is subject to limitations of the CXR modality compared to echocardiography or CT. As demonstrated in case 4 (ASD) and cases 6 and 7 (mediastinal mass), CVBs can be influenced by adjacent structures. Therefore, the interpretation of CVB analysis must be based on understanding of the specific disease's pathophysiology and topographical anatomical knowledge in CXR. Second, although this study presents diagnostic performance, *z*-score pattern analysis, and prognostic value, it has not provided definitive cutoff values refined enough for application in actual practice. This is because, although the normal ranges and disease cohorts included data from multiple institutions, they did not encompass a wide variety of ethnicities and real-world conditions, including disease groups. Future research should conduct more extensive studies across a wide range of clinical application scenarios. Third, while we utilized diverse data sets from Korea and America to establish normal values for CVB analysis, we were unable to perform an analysis of detailed race composition. Lastly, our AI model's performance has not been sufficiently validated in real-world clinical settings that accurately reflect disease prevalence. Future prospective studies using consecutively enrolled, disease-specific data that truly reflect prevalence will be necessary for further validation.

The ADC study has introduced a fully automated, deep learning-derived *z*-score analysis of CXR showed potential in detecting, classifying, and stratifying the risk of cardiovascular abnormalities. Further research is needed to determine the most beneficial clinical scenarios for this method.

ACKNOWLEDGMENTS Prof Tae-Hwan Lim provided critical feedback, expertise, and encouragement for the ADC study.

FUNDING SUPPORT AND AUTHOR DISCLOSURES

This research was supported by a grant of the Korea Health Technology R&D Project through the Korea Health Industry Development Institute (KHIDI), funded by the Ministry of Health & Welfare, Republic of Korea (grant number: HR20C0026). Drs Yang and J. G. Lee reported holding a U.S. patent (11783477 B2) related to this work. All other authors have reported that they have no relationships relevant to the contents of this paper to disclose.

ADDRESS FOR CORRESPONDENCE: Dr Dong Hyun Yang, Department of Radiology, Asan Medical Center, University of Ulsan College of Medicine, 88, Olympic-ro 43-gil, Songpa-gu, Seoul 05505, South Korea. E-mail: donghyun.yang@gmail.com OR donghyun.yang@amc.seoul.kr. OR Dr Young-Hak Kim, Department of Cardiology, Asan Medical Center, University of Ulsan College of Medicine, 88, Olympic-ro 43-gil, Songpa-gu, Seoul 05505, South Korea. E-mail: mdyhkim@amc.seoul.kr.

PERSPECTIVES

COMPETENCY IN MEDICAL KNOWLEDGE: This study demonstrates that deep learning-based quantification of CVBs in CXRs can provide objective, reproducible measurements that go beyond the traditional CT ratio. By establishing age- and sex-specific normal ranges and standardizing values into *z*-scores, our approach improves the detection of valve disease and offers prognostic insights in CAD. Understanding these imaging biomarkers is crucial for enhancing diagnostic accuracy and risk stratification in cardiovascular care.

TRANSLATIONAL OUTLOOK: Our findings suggest that automated, deep learning-derived *z*-score analysis of CVBs has the potential to transform clinical practice by streamlining CXR interpretation and improving patient management. Future prospective studies in diverse populations are necessary to validate these findings and integrate the technology into clinical workflows. Ultimately, such advancements may lead to earlier detection and more targeted interventions for cardiovascular diseases.

REFERENCES

1. Yun J, Ahn Y, Cho K, et al. Deep learning for automated triaging of stable chest radiographs in a follow-up setting. *Radiology*. 2023;309:e230606.

2. Hwang EJ, Park CM. Clinical implementation of deep learning in thoracic Radiology: potential applications and challenges. *Korean J Radiol*. 2020;21:511-525.

3. Wu K, Wu E, Theodorou B, et al. Characterizing the clinical adoption of medical AI devices through U.S. Insurance claims. *NEJM AI*. 2024;1:AIoa2300030.

4. D'Ancona G, Massussi M, Savardi M, et al. Deep learning to detect significant coronary artery disease from plain chest radiographs AI4CAD. *Int J Cardiol*. 2023;370:435-441.

5. Ueda D, Matsumoto T, Ehara S, et al. Artificial intelligence-based model to classify cardiac functions from chest radiographs: a multi-institutional, retrospective model development and validation study. *Lancet Digit Health*. 2023;5:e525-e533.

6. Hsiang CW, Lin C, Liu WC, et al. Detection of left ventricular systolic dysfunction using an artificial intelligence-enabled chest X-ray. *Can J Cardiol*. 2022;38:763-773.

7. Bhave S, Rodriguez V, Poterucha T, et al. Deep learning to detect left ventricular structural abnormalities in chest X-rays. *Eur Heart J*. 2024;45:2002-2012.

8. Weiss J, Raghu VK, Paruchuri K, et al. Deep learning to estimate cardiovascular risk from chest radiographs : a risk prediction study. *Ann Intern Med*. 2024;177:409-417.

9. Arun N, Gaw N, Singh P, et al. Assessing the trustworthiness of saliency maps for localizing abnormalities in medical imaging. *Radiol Artif Intell*. 2021;3:e200267.

10. Libby P. Braunwald's heart disease : a textbook of cardiovascular medicine. Twelfth edition ed. Amsterdam: Elsevier; 2021.

11. Yang DH, Seo JB, Lee IS, et al. Displaced aortic arch sign on chest radiographs: a new sign for the detection of a left paratracheal esophageal mass. *Eur Radiol*. 2005;15:936-940.

12. Kim C, Lee G, Oh H, et al. A deep learning-based automatic analysis of cardiovascular borders on chest radiographs of valvular heart disease: development/external validation. *Eur Radiol*. 2022;32:1558-1569.

13. Wang X, Peng Y, Lu L, Lu Z, Bagheri M, Summers RM. ChestX-Ray8: Hospital-Scale Chest X-Ray Database and Benchmarks on Weakly-Supervised Classification and Localization of Common Thorax Diseases. In: *2017 IEEE Conference on Computer Vision and Pattern Recognition (CVPR)*: *IEEE Computer Society*: Washington, DC. 2017:3462-3471.

14. Irvin J, Rajpurkar P, Ko M, et al. Chexpert: a large chest radiograph dataset with uncertainty labels and expert comparison. *Proc AAAI Conf Artif intelligence*. 2019;73:590-597.

15. Ahn I, Na W, Kwon O, et al. CardioNet: a manually curated database for artificial intelligence-based research on cardiovascular diseases. *BMC Med Inform Decis Mak*. 2021;21:29.

16. Cho MS, Roh JH, Park H, et al. Practice pattern, diagnostic yield, and long-term prognostic impact of coronary computed tomographic angiography. *J Am Heart Assoc*. 2020;9:e016620.

17. Rigby RA, Stasinopoulos DM. Using the Box-Cox t distribution in GAMLSS to model skewness and kurtosis. *Stat Model*. 2006;6:209-229.

18. Kac G, Carilho TRB, Rasmussen KM, et al. Gestational weight gain charts: results from the Brazilian maternal and child nutrition consortium. *Am J Clin Nutr*. 2021;113:1351-1360.

19. Saiviroonporn P, Rodbangyang K, Tongdee T, et al. Cardiothoracic ratio measurement using artificial intelligence: observer and method validation studies. *BMC Med Imaging*. 2021;21:95.

20. Kim D, Lee JH, Jang MJ, et al. The performance of a deep learning-based automatic measurement model for measuring the cardiothoracic ratio on chest radiographs. *Bioengineering (Basel)*. 2023;10:1077.

21. Thiam P, Kloth C, Blaich D, Liebold A, Beer M, Kestler HA. Segmentation-based cardiomegaly detection based on semi-supervised estimation of cardiothoracic ratio. *Sci Rep*. 2024;14:5695.

22. Fan W, Yang Y, Qi J, et al. A deep-learning-based framework for identifying and localizing multiple abnormalities and assessing cardiomegaly in chest X-ray. *Nat Commun*. 2024;15:1347.

23. Raghu VK, Weiss J, Hoffmann U, Aerts H, Lu MT. Deep learning to estimate biological age from chest radiographs. *JACC Cardiovasc Imaging*. 2021;14:2226-2236.

24. Kolossvary M, Raghu VK, Nagurney JT, Hoffmann U, Lu MT. Deep learning analysis of chest radiographs to triage patients with acute chest pain syndrome. *Radiology*. 2023;306:e221926.

25. Lee DK, Kim JH, Oh J, et al. Detection of acute thoracic aortic dissection based on plain chest radiography and a residual neural network (Resnet). *Sci Rep*. 2022;12:21884.

26. Ueda D, Yamamoto A, Ehara S, et al. Artificial intelligence-based detection of aortic stenosis from chest radiographs. *Eur Heart J Digit Health*. 2022;3:20-28.

27. Matsumoto T, Ehara S, Walston SL, Mitsuyama Y, Miki Y, Ueda D. Artificial intelligence-based detection of atrial fibrillation from chest radiographs. *Eur Radiol*. 2022;32:5890-5897.

28. Yuyun MF, Sliwa K, Kengne AP, Mocumbi AO, Bukhman G. Cardiovascular diseases in sub-saharan Africa compared to high-income countries: an epidemiological perspective. *Glob Heart*. 2020;15:15.

KEY WORDS artificial intelligence, cardiovascular borders, cardiovascular disease detection, chest x-rays

APPENDIX For an expanded Methods section, supplemental tables and figures, please see the online version of this paper.